

# Measurement and Visualization of Loudspeaker Cone Vibration

Wolfgang Klippel<sup>1</sup> and Joachim Schlechter<sup>2</sup>

<sup>1</sup> Klippel GmbH, Dresden, 01277, Germany  
klippel@klippel.de

<sup>2</sup> Faculty of Computer Science, University of Technology, Dresden, Germany  
js571054@inf.tu-dresden.de

## ABSTRACT

Optical measurement of loudspeaker cone vibration (scanning vibrometry) can also be accomplished by using Laser triangulation technique which is a cost effective alternative to Doppler interferometry. Since triangulation sensors provide primarily displacement advanced signal processing is required to measure the break-up modes up to 20 kHz at sufficient signal to noise ratio. In addition to stroboscopic animation of the radiation pattern a new decomposition technique is presented for the visualization of the measured data. Radial and circular modes can be separated and the total vibration can be split into radiating and non-radiating vibration components. This kind of post-processing reveals critical vibration modes, simplifies the interpretation and gives indications for further improvements.

## 1. INTRODUCTION

Analysing the sound pressure produced by a loudspeaker driver means to investigate a complex interaction of cone vibration patterns and sound radiation. A measurement of these vibrations leads to a multitude of information at each frequency where the essential contribution of the vibrations to the final sound pressure might not be evident.

Thus, it is the goal of this paper to develop an effective analysis method which allows an easy interpretation of the loudspeaker behaviour. Focussing only on the vibration information which is significant for the produced sound pressure simplifies the analysis and supports a better understanding of the physical mechanisms involved.

The paper is divided into the following sections:

First, a simple and cost-effective technique for vibration measurements is introduced on the basis of a triangulation laser device. Afterwards, appropriate post-processing and visualization methods are implemented allowing an efficient interpretation of the measured data. Finally the practical aspects of such an interpretation are presented for an example driver.

## 2. VIBROMETRY

Vibrometry is the technique of measuring mechanical vibrations, see Fig. 21.

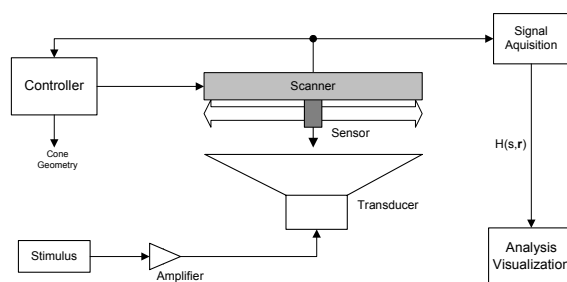


Fig. 1: Vibrometry of an electroacoustical transducer.

Vibrations can be expressed in terms of displacement, velocity or acceleration which can be easily transformed into each other. In comparison to the Laser Doppler Vibrometry where the actual velocity of a moving surface is measured, in this paper a different approach is considered measuring the displacement with a triangulation laser.

## 2.1. Sensing Displacement

The voice coil displacement falls at 12 dB per octave above resonance frequency where the mass is dominant. Thus a sinusoidal sweep with constant voltage generates  $x_{\text{peak}}(f_s) = 1 \text{ mm}$  at the resonance frequency  $f_s = 20 \text{ Hz}$  but would produce only  $10^{-6} \text{ mm}$  (1nm) peak displacement at 20 kHz.

Measurement of the displacement at higher frequencies with reasonable signal to noise ratio can be accomplished by using the technique shown in Fig. 2.

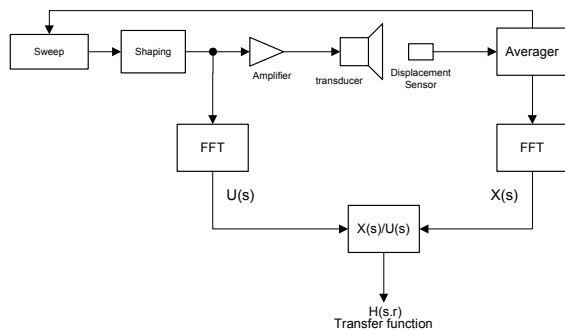


Fig. 2: Measurement of the displacement transfer function at high signal to noise ratio.

## 2.2. Shaping of the Stimulus

The decay of the displacement above resonance frequency can be compensated by using a stimulus where the higher frequency components are emphasized inversely. For example Fig. 3 shows a sinusoidal sweep signal where the instantaneous frequency varies logarithmically from 100 Hz to 10 kHz. The amplitude is not constant but rises quadratically with frequency from 0.1 mV up to 10 V rms.

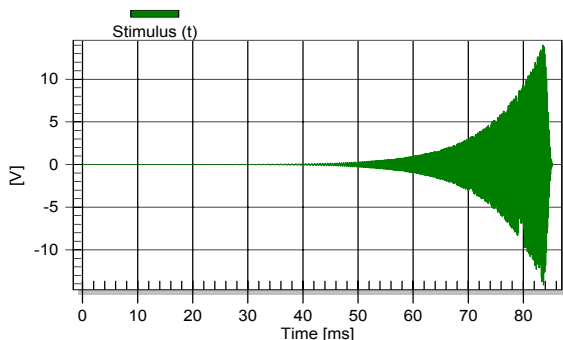


Fig. 3: Shaped logarithmic sinusoidal sweep used as stimulus.

The spectrum of the stimulus is presented in Fig. 4. The sweep time of about 100 ms produces distinct frequency components at a distance of about 10 Hz giving sufficient resolution at higher frequencies. The amplitude profile and the logarithmic sweep speed results in a shaping of the frequency components rising with 12 dB per octave.

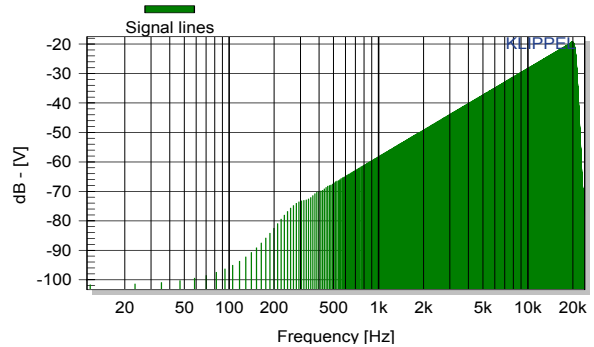


Fig. 4: Spectrum of the shaped logarithmic sine sweep.

## 2.3. Repetitive Measurement

Repeating the measurements with the same stimulus  $2^n$  times and averaging the measured displacement responses will improve the signal to noise ratio by  $3 \cdot n \text{ dB}$ . Since a single sweep is relatively short extensive averaging (e.g. 128) can be applied improving the SNR by more than 20 dB.

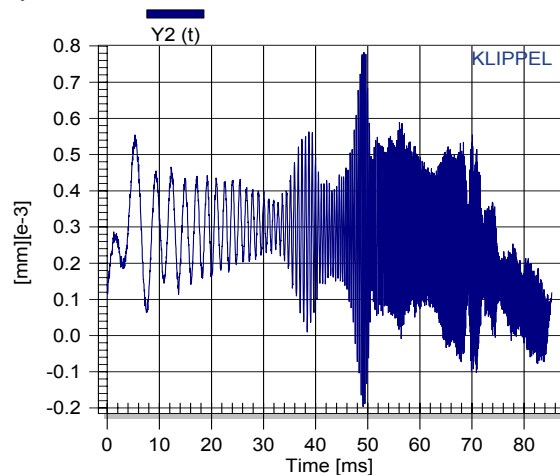


Fig. 5: Averaged displacement signal measured by using a triangulation laser.

For example, Fig. 5 and Fig. 6 show the averaged response in the time and frequency domain, respectively. Due to the shaping of the stimulus the displacement at the resonance (about 100 Hz) is in the same order of magnitude (about  $0.5 \mu\text{m}$ ) as at high

frequencies. The noise floor measured separately in a second measurement without stimulus stays at 5nm giving sufficient signal to noise ratio (> 40 dB) as shown in Fig. 6.

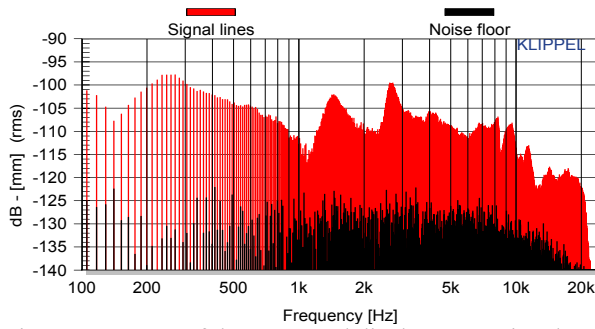


Fig. 6: Spectrum of the measured displacement signal compared with the noise floor.

The high peak voltage at the end of the sinusoidal sweep may operate the transducer in the large signal domain causing nonlinear distortion in the sound pressure output. However, available triangulation sensors are not sensitive enough to measure the distortion in the displacement. Due to the high crest factor of the stimulus the total power supplied to the transducer is small. A significant heating of the coil which changes the resistance  $R_e$  and other indications of mechanical overload have not been observed.

## 2.4. Displacement Transfer Function

Due to the shaping of the stimulus the output signal of the triangulation laser corresponds with the acceleration of the target point. Since the shaping is not relevant for further analysis it is more convenient to calculate the transfer function  $H(s,r)=X(s)/U(s)$  by referring the displacement  $X(s)$  to the voltage  $U(s)$  of the stimulus. For example, the amplitude and phase response of  $H(s,r)$  measured in the center of the dust cap and at one point of the surround are presented in Fig. 7 and Fig. 8, respectively.

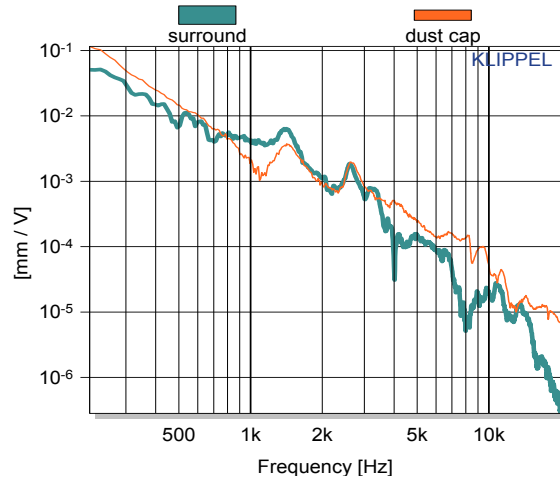


Fig. 7: Magnitude response of the transfer function  $H_x(s)=X(s)/U(s)$  between voltage  $U(s)$  and displacement  $X(s)$  measured at the dust cap and at the surround.

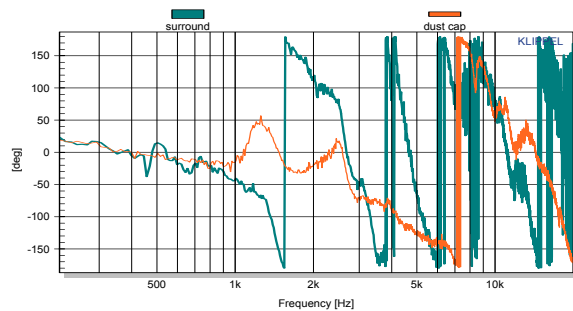


Fig. 8: Phase response of the transfer function  $H_x(s)=X(s)/U(s)$  between voltage  $U(s)$  and displacement  $X(s)$  measured at the dust cap and at the surround.

Below 1 kHz both points vibrate in-phase which is typical for the piston mode. However, the magnitude of the vibration is significantly higher at the dust cap than in the middle of the corrugation roll. The amplitude response reveals a distinct resonance at 1.5 kHz where both points vibrate in anti-phase at almost the same amplitude. The first cone break-up mode occurs at 3 kHz where again both points vibrate in phase. At higher frequencies the dust cap has a higher amplitude than the surround.

## 3. SCANNING METHOD

The manual measurement of the vibration at a few points on the target surface may be sufficient for detecting the surround resonance and severe rocking modes but is usually not sufficient to analyze break-up modes with an adequate spatial resolution at higher frequencies.

In this section an automatic method for scanning mechanical vibration is developed which considers the particularities of the object under test applying a displacement sensor based on the laser triangulation principle.

### 3.1. Laser Triangulation Principle

The laser triangulation sensors got their name from the fact that the sensor enclosure, the emitted and the reflected laser beam form a triangle as shown in Fig. 9.

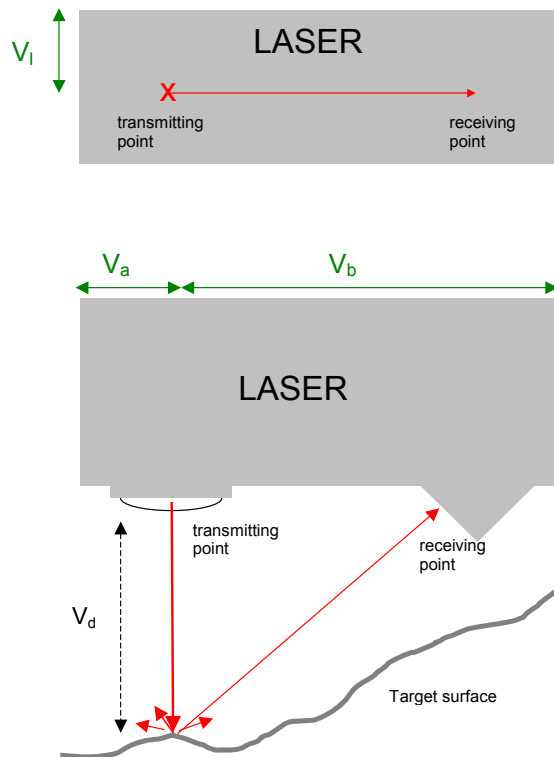


Fig. 9: Laser displacement sensor based on the triangulation principle.

The laser beam is emitted at the transmitting point and is reflected from the target surface to a collection lens. The receiving point is typically located adjacent to the laser emitter but views the target point from an angle that varies from 45 to 65 degrees at the center of the measurement range. The lens focuses an image of the spot on a linear CCD array element and the position of the spot image on the pixels of the CCD element is then processed to determine the distance to the target. The beam is viewed from one side so that the apparent location of the spot changes with the distance to the target.

The triangulation principle causes the following particularities which are important for a scanning application:

1. The laser sensor has to be placed at a certain distance  $V_d$  from the target surface to measure maximal positive and negative peak displacement  $\pm X_{\text{peak}}$  of the target. The higher the sensitivity of the laser, the smaller is the useable measurement range  $-X_{\text{peak}} < x < X_{\text{peak}}$  and the smaller the distance  $V_d$  between sensor head and target. However, a distance  $V_d$  of about 30 mm may be considered as a good compromise between sensitivity, measurement range and positioning of the laser head.
2. The triangulation principle requires a certain size of the laser head with the implication that the sensor can not optimally be adjusted at certain geometries (e.g. narrow gaps) on the target surface. The distances  $V_a$ ,  $V_b$  and  $V_i$  between the transmitting point and the edges of the enclosure as defined in Fig. 9 have to be considered in the automatic control of the mechanical scanning system.

### 3.2. Mechanical Scanning System

Most electro-acoustical transducers use a single motor which excites the diaphragm, cone or panel in one direction (z dimension). Thus the measurement of the displacement in this direction is sufficient in loudspeaker applications. This can be accomplished by using one displacement sensor scanning 2 dimensions (radius  $r$  and angle  $\varphi$ ) of the target surface. Instead of moving the sensor the transducer under test is rotated by a turn table ( $\varphi$  coordinate) and shifted by a linear actuator ( $r$  coordinate). An additional actuator is required to adjust the laser to the optimal distance  $V_d$  in the z dimension. Such a mechanical can be realized by using three step motors, an electronic control system and a robust mechanical frame as illustrated in Fig. 10.

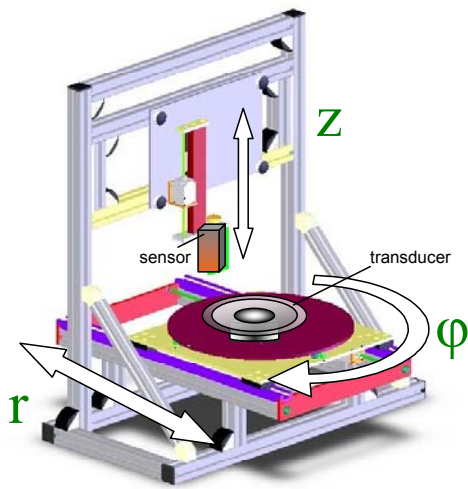


Fig. 10: Mechanical scanning system with one rotational ( $\phi$ ) and two linear actuators ( $r$ ,  $z$ ).

### 3.3. Scanning Scheme

The way the sensor is moved relatively to the target surface is important for the speed and the robustness of the scanning process. Clearly the time for moving to the next measurement point is minimal if adjacent points at approximately the same height ( $z$  coordinate) are measured immediately one after another. This leads to cyclic scan paths starting outside at the surround or at the center of the dust cap as illustrated in Fig. 11.

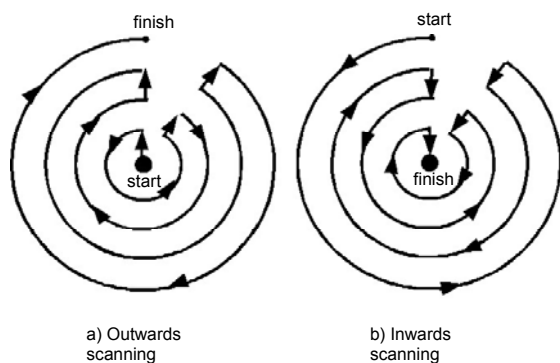


Fig. 11: Alternative scanning paths on the target surface.

While moving on the scanning path the transfer function  $H(r_i, s)$  is measured at a particular point  $r_i$  on the scanning grid. The distance between the measurement points  $r_i$  limits the local resolution of the scan and the capability to identify higher-order modes without aliasing effects. An equidistant grid may be generated automatically. However, it is useful to increase the

measurement points manually at critical areas such as the outer suspension or the dust cap.

Since the laser sensor has to be adjusted close to the target surface (about 30 mm) precaution have to be taken to avoid a mechanical contact and damage of either sensor or transducer. While the shape of the target surface is unknown the geometry of the sensor can be used to guide the sensor safely on the target surface.

The orientation of the laser head and the starting point are crucial to realize robust scanning techniques. Three alternative methods are interesting:

#### 3.3.1. Out-lateral Scan

Before starting the scanning process the laser point is adjusted manually to the center of the target surface (dust cap or inner ring of the cone if a phase plug is used). The laser head is mounted in **lateral** orientation where the plane of the laser beam triangle is perpendicular to the scanning direction as shown in Fig. 12. During the scanning process the laser head is moved **outwards** while laser transmitting point is always ahead of the receiving point. Most parts of the laser enclosure are always above identified areas of the target surface. A sophisticated control algorithm always calculates the distance to the target and skips the measurement at a particular point automatically to avoid a collision. The edge of the laser head at the distance  $V_a$  in front of the transmitting point limits the scanning of some geometries having a steep slope.

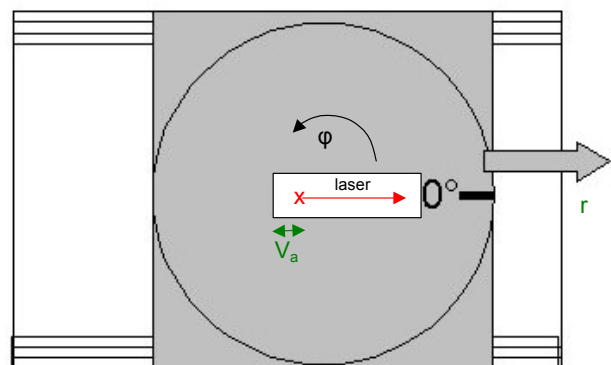


Fig. 12: **Outwards** scanning scheme starting at the centre with **lateral** laser orientation (OUT-LATERAL).

#### 3.3.2. In-lateral Scan

An alternative scanning scheme shows Fig. 13 where also the lateral laser orientation is used but the scan path starts at the outer rim of the target surface and moves inwards to the center. Again the laser transmitting point

is always ahead of the receiving point to predict a collision with the rear part of the laser.

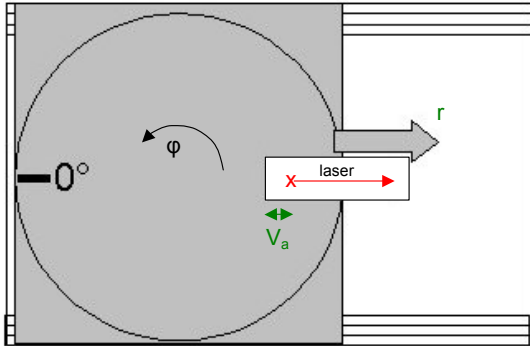


Fig. 13: Inwards scanning scheme starting at the outer rim with **lateral** laser orientation (IN-LATERAL).

### 3.3.3. In-frontal Scan

Turning the laser head by  $90^\circ$  gives the third scanning scheme as shown in Fig. 14. Here the receiving point will not follow the path of the transmitting point. However, most transducers have an axial-symmetrical shape where the geometrical information measured at a particular radius can be applied to any angle of the circle. By starting at the outer rim and scanning inside the distance below the rear part of the laser can be predicted from data collected in previous measurements with higher radius  $r$ . The half thickness of the laser head  $V_l$  is the laser dimension which limits the scanning of surfaces having a steep slope.

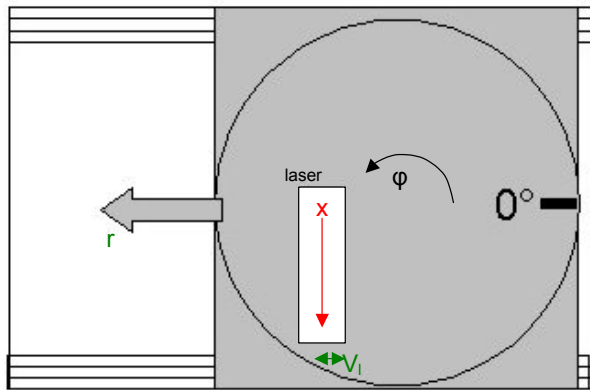


Fig. 14 Inwards scanning scheme starting at the outer rim with **frontal** laser orientation (IN-FRONTAL).

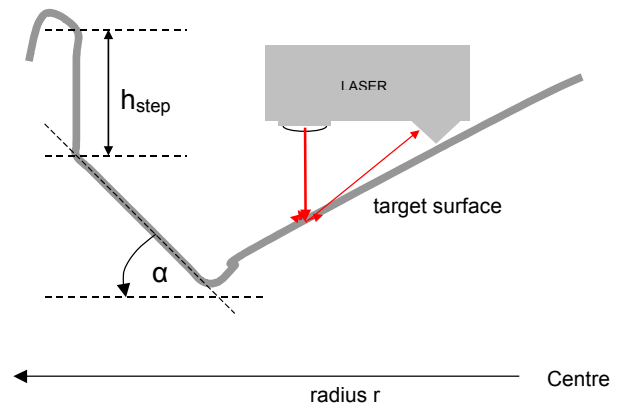


Fig. 15: The geometry of the target surface (e.g. steep slope) may impair the scanning of a particular point.

### 3.4. Limitations

The scanning technique has the following limitations:

- Similar to the Doppler interferometry the target surface should be freely accessible in the dimension ( $z$ ) in which the vibration is measured. Thus the vibration of a spider or voice coil former which are usually covered by a cone are not accessible.
- Due to the triangulation principle the size of the sensor ( $V_a+V_b$ ) is not small in comparison to the measurement distance  $V_d$ . Thus the sensor may fail at a target surface with a narrow gap such as a tweeter cone used in full band loudspeakers.
- There are also some limits related with the profile of a non even target surface. The triangulation sensor can cope with any abrupt variations of the  $z$  dimension if the height  $h_{step}$  of the step is below the laser dimension  $V_d$  as illustrated in Fig. 15. For larger variations the slope should be below a critical angle  $\alpha$  depending on the geometry and orientation of laser

$$\alpha_a = \cot\left(\frac{V_a}{V_d}\right) \quad (0.1)$$

$$\alpha_b = \cot\left(\frac{V_b}{V_d}\right) \quad (0.2)$$

$$\alpha_l = \cot\left(\frac{V_l}{V_d}\right) \quad (0.3)$$

Since the dimension  $V_a \ll V_b$  a triangulation laser can better cope with steep slopes if the transmission point is oriented towards the higher side of the slope. Thus the OUT-LATERAL scanning scheme is able to scan a steep cone (positive angle) but not a dust cap having the same steepness but falling in the opposite direction (negative angle) as shown in Table 1. The IN-LATERAL scheme has just the inverse behavior and can measure high negative angles as found on the slope of a steep dust cap. The combination of both techniques can measure slopes up to the maximal positive and negative slope angle  $\pm\alpha_a$ . If the loudspeaker has an axially symmetric design and is carefully centered on the turn table, the two LATERAL scanning schemes (IN- and OUT-LATERAL) can be performed one after another without changing the laser orientation.

Scanning Scheme	Maximal angle $\alpha$ of surface slope	Maximal Step size $h_{\text{step}}$ of surface slope
OUT-LATERAL	$-\alpha_b < \alpha < \alpha_a$ ( $-31^\circ < \alpha < 68^\circ$ )	$h_{\text{step}}=V_d$ (30 mm)
IN-LATERAL	$-\alpha_a < \alpha < \alpha_b$ ( $-68^\circ < \alpha < 31^\circ$ )	$h_{\text{step}}=V_d$ (30 mm)
IN-FRONTAL	$-\alpha_l < \alpha < \alpha_l$ for $r > V_a$ ( $-68^\circ < \alpha < 68^\circ$ )	$h_{\text{step}}=V_d$ (30 mm)

Table 1: Limit angle of the scanning schemes (using  $V_d=30$  mm,  $V_B=50$  mm,  $V_a=12$  mm,  $V_l=12$  mm).

The IN-FRONTAL scanning scheme as shown in Fig. 14 can scan target surfaces with a high positive or negative slope angle  $\pm\alpha_l$  directly as long as the steep slope of the target surface is located in the outside region ( $r > V_B$ ). Close to the centre ( $r < V_B$ ) the back part of the laser is limited by a positive slope angle of  $\alpha_b$ . However, many loudspeaker systems have a relatively flat dust cap where the IN-FRONTAL scanning scheme is the most powerful technique.

### 3.5. Practical Measurements

Although the scanning process is completely automated the preparation of the scanning process requires only few actions from the user:

- Input of the maximal diameter of the cone, and density of the scanning grid.
- Centering and clamping of the loudspeaker on the turntable.
- Connecting the terminals to the cables providing the stimulus.

After adjusting the laser sensor manually to the starting point of the scanning path the measurement is started. The control software guides the laser head on the

scanning path as shown in Fig. 11, performs the measurement of the transfer function  $H(r_i, s)$  at each measurement point  $r_i$  on the grid and stores the data in a separate file. The positioning of the laser sensor to the next point and performing one transfer function measurement takes about 5 – 10 s. Thus complete measurements at high resolution (1000 points) can usually take multiple hours. The progress of the measurement is shown in the control software. The measurement can be interrupted at any time and continued with a different grid to adjust the resolution to the special requirements.

## 4. VISUALIZATION AND ANALYSIS

The measured transfer functions at each scanning point contain a huge amount of complex vibration data. The task for a practical post-processing of the measurements is therefore to bring out the relevant information and to provide helpful tools to analyze the vibration and radiation properties of the considered loudspeaker.

### 4.1. Image Processing

A first step for the visualization of the vibrations is to create a complete picture from the measurement data. At each measured frequency a 3-dimensional picture of the loudspeaker vibration can be composed displaying amplitude and phase of the transfer functions. Due to the fact that the laser scanner might not be able to measure all specified scan points an interpolation of not-measured data is desirable to fill the gaps in the data.

To increase the visual quality of the vibration picture also additional points within the measured grid can be interpolated. An optional smoothing of the measurement data can help to remove noise and vibrations of low amplitude to get a simplified image focusing on the main vibration shape.

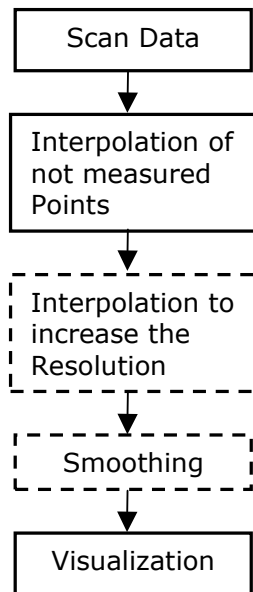


Fig. 16: The data interpolation scheme with optional increase of resolution and smoothing.

Because the triangulation laser provides the geometry of the loudspeaker cone, a 3-dimensional surface of the cone can be created. This surface serves as rest position and the amplitude of the vibration is displayed as an offset superposing the geometry including a certain scaling to emphasize small movements.

#### 4.1.1. Amplitude Coloration

Not only the geometry of the 3D object but also the color of the faces can be utilized to display information about the vibration in a quickly comprehensible way.

A first way of coloration is based on the amplitude of the vibration. A positive amplitude is correlated with a blue color and a negative amplitude with a red color while neutral points remain white. The intensity of the coloration expresses the magnitude of the vibration in relation to the maximal amplitude on the complete surface. That means the point with the highest amplitude will be colored in strong blue or red while a point with little amplitude will get only a lightly shimmering blue or red tone. All points where the laser could not measure vibration data are indicated by a neutral gray color to emphasize that these points are only interpolated and may not exactly represent the actual vibration.

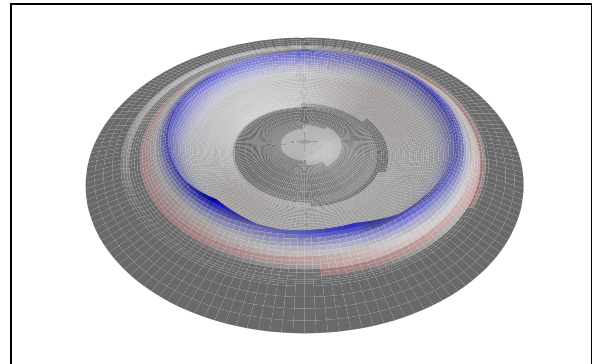


Fig. 17: Amplitude coloration of the vibration at 2kHz.

By this type of coloration it is very easy to see, which regions on the loudspeaker membrane vibrate with a high motional amplitude.

#### 4.1.2. Phase Coloration

By an alternative coloration scheme only the phase of the vibration determines the color. A phase angle of zero corresponds now to the color yellow and the opposite phase of  $180^\circ$  is represented by a red color. In between these both phases a smooth color transition is established. The advantage of this coloration is that even vibrations of small amplitude will be clearly visible. The spatial shape of the vibration appears more clearly which helps to determine the involved vibration modes.

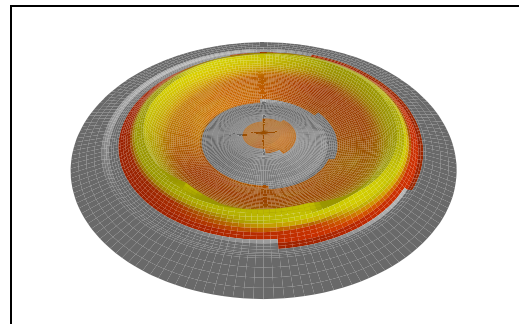


Fig. 18: Phase coloration of the vibration at 2 kHz.

Both coloration modes complement each other and can be quickly switched to support a good understanding of the measured vibrations.

## 4.2. Animation as Stroboscopic Movie

A graphical animation can illustrate the behavior of the cone vibrations in a very good way. If single pictures are displayed at a rate higher than about 24 frames per second (*fps*), then the human eye interprets the picture sequence as a continuous motion. A way of animating a vibration is to rotate the phase angle of all points by 360° during one animation period. The period time  $T$  can be chosen freely to slow down the vibration until a good understanding of the animation is possible.

To calculate the single frames  $n$  of the animation for each point on the 3D surface the phase has to be changed by small steps.

$$\bar{x}_n = \hat{x} e^{j\left(\varphi_x + \frac{2\pi T}{f_{ps}} n\right)} \quad (0.4)$$

Obviously this calculation can become quite time-consuming the more points have to be recalculated. If the calculation of the frames takes more time than the animation frame rate allows, a visible delay and flickering in the animation will occur. Therefore a compromise has to be found between the number of displayed points and a fluent animation.

This restriction can be circumvented by calculating all necessary pictures first and then creating a movie file from the calculated pictures. Now the calculations do not have to be done in real-time and also a higher number of points can be used while keeping a fluent animation.

The movie file can be stored in the AVI format, which is a common file format for video streams. By this also a storage of certain vibration animations is possible which allows i.e. the comparison of the effects of certain changes in the loudspeaker design.

## 4.3. Prediction of the Sound Pressure Output

On the basis of the measured vibration data a modeling of the radiated sound pressure is possible. As the produced sound is of final interest in the loudspeaker design a directly available model of the sound pressure is a helpful assistance.

### 4.3.1. Frequency Response

Several acoustical models can describe the relation between the velocity of a vibrating surface and the radiated sound pressure. These models differ regarding their accuracy and limitations. A simple point source

model is used in the actual visualization software, which can easily be exchanged by more advanced boundary element models (BEM) in the future.

The implemented point source model places a monopole sound source at each measured point on the surface. The sound pressure at a certain model point in the space in front of the speaker is then simply the summation of the radiation of all point sources on the surface.

Equation (0.5) shows the relation between the measured displacement  $\bar{x}(\vec{r}_s) = \hat{x}(\vec{r}_s) e^{j\varphi_x(\vec{r}_s)}$  at each point  $\vec{r}_s$  on the surface and the total radiated sound pressure  $p$ .

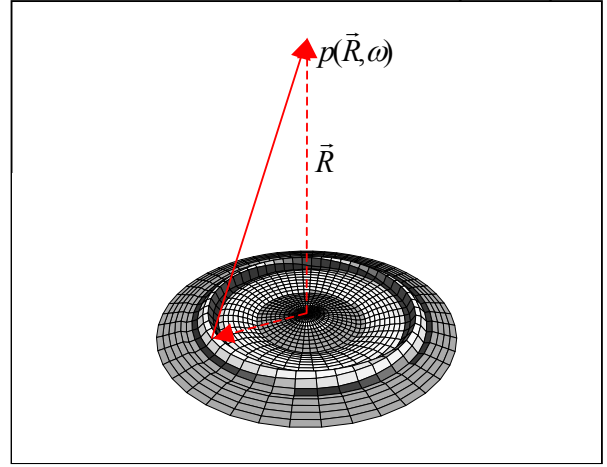


Fig. 19: Sound pressure modeling.

$$\bar{p}(\vec{R}, \omega) = \frac{-\omega^2 \rho_0}{2\pi} \int_S \frac{\hat{x}(\vec{r}_s)}{|\vec{R} - \vec{r}_s|} e^{j(\varphi_x(\vec{r}_s) - k_0 |\vec{R} - \vec{r}_s|)} dS \quad (0.5)$$

There are a couple of assumptions under which this model is valid only. First, the loudspeaker is assumed to vibrate in an infinite rigid baffle. Furthermore, only the sound pressure in the far field of the loudspeaker can be modeled, that means at points in great distance from the surface. This model also neglects the influence of the moved air in front of the diaphragm, which does have an effect especially at low frequencies.

To get a model for the frequency response of the loudspeaker the sound pressure is finally evaluated at the model point for each measured frequency.

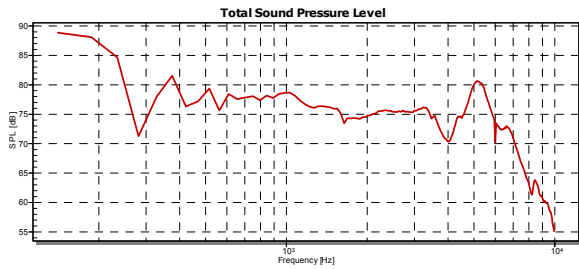


Fig. 20: Modeled sound pressure level in axis.

### 4.3.2. Directivity Pattern

The same modeling technique can also be used to calculate the directivity of the loudspeaker. For this the sound pressure is evaluated at one certain frequency for several model points on a hemisphere around the speaker.

The sound pressure model can not give exact results, when some regions of the loudspeaker cone are shaded by other regions. That means there is a certain maximal opening angle  $\theta_{max}$  determined by the cone geometry wherein the model is valid.

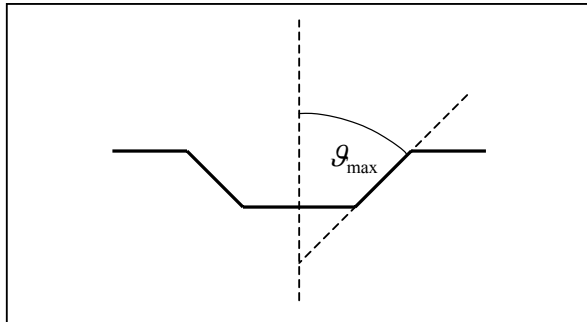


Fig. 21: Maximal valid opening angle for sound pressure modeling.

Whereas directivity plots usually assume an axially symmetric radiation of the speaker, our model allows to precisely look at a certain angle  $\varphi$  above the speaker surface to detect possible asymmetries in sound radiation.

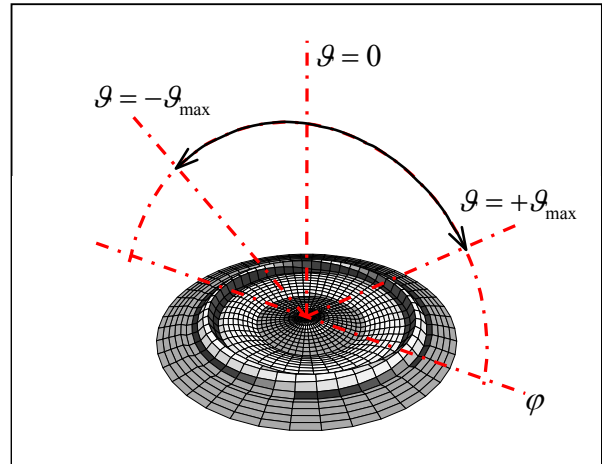


Fig. 22: Evaluation points for directivity plots.

The final directivity plot in Fig. 23 shows the modeled sound pressure level for a certain frequency and angle  $\varphi$  at several points in between the maximal valid opening range.

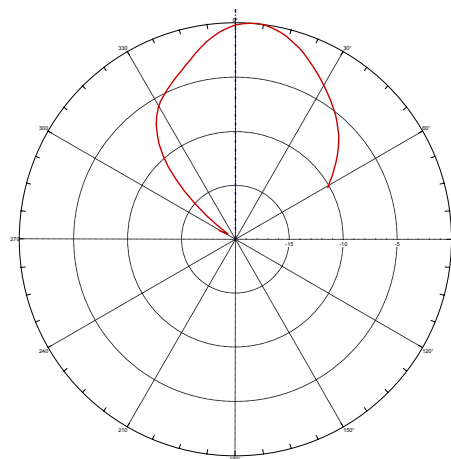


Fig. 23: Directivity of the total vibration at 7640 Hz.

### 4.4. Decomposition

The 3D-animation provides a good image of the total cone vibration at a certain frequency. To analyze the vibrational behavior more in detail it is possible to decompose the total motion into independent vibration components with different properties.

For the mechanical analysis of the cone vibrations a decomposition into radial and circular components can

help to separate the influence of certain vibration modes. Another interesting analysis opportunity is to separate vibration components according to their relation regarding the finally radiated sound.

#### 4.4.1. Radial and Circular Modes

A separation into vibration components propagating in radial direction and components propagating in circular direction is especially useful for axis-symmetric cones. Then both propagation directions refer to independent mechanical vibration modes which do not interfere with each other.

$$\bar{x}_{total} = \bar{x}_{rad} + \bar{x}_{circ} \quad (0.6)$$

Theoretically, circular vibrations should hardly occur in loudspeaker cones, because they are not excited by a symmetrically moving voice coil. But in praxis small irregularities will also lead to some circular motions in the cone. This component is usually quite small in comparison to the radial motion and might therefore be hardly visible looking only at the total vibration.

The decomposition is implemented by an averaging of the vibrating points along each radius on the cone surface. Projecting this average value on all points along the respective radius gives the radial vibration component.

$$\bar{x}_{rad}(r, \varphi) = \frac{1}{n} \sum_{i=1}^n \bar{x}_{total}(r, \varphi_i) \quad (0.7)$$

The remaining circular vibration component is obtained by subtracting the radial component from the total vibration.

$$\bar{x}_{circ} = \bar{x}_{total} - \bar{x}_{rad} \quad (0.8)$$

According to Frankort [1], the circular vibration components have a negligible effect on the total radiated sound. Therefore the simplification of the vibration picture by considering only the radial component should maintain the sound radiation properties while showing an easier understandable picture of the cone vibrations.

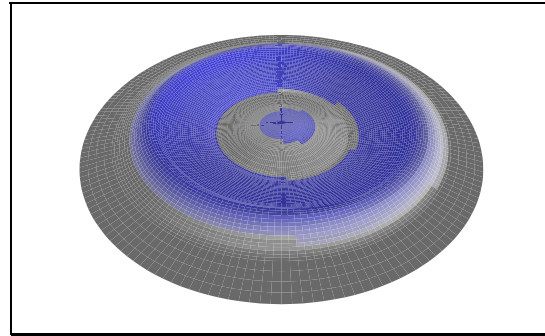


Fig. 24: Radial component at 375Hz.

On the other hand considering only the circular vibration component can reveal asymmetric vibrations which while not contributing much to the radiated sound nevertheless can introduce distortion due to rubbing of the voice coil in the gap. The reason for these asymmetric vibrations can be a non-symmetric mass distribution of the voice coil or the cone.

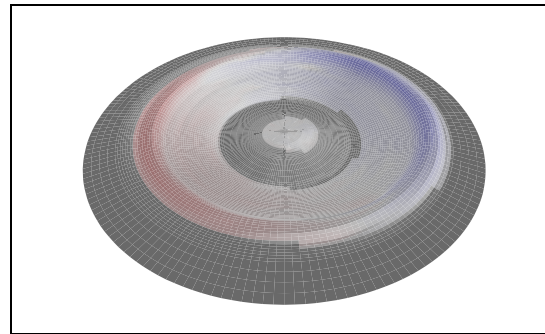


Fig. 25: Circular component at 375Hz.

Furthermore the circular components can still have some effect on the sound pressure considering radiation regions aside the centered loudspeaker axis. A circular cone vibration mode will usually lead to a multipole (dipole, quadrupole,...) radiation pattern with little radiated sound pressure in axis but radiating side lobes.

It has to be noted, that this kind of vibration decomposition presumes an accurate centering of the speaker on the turntable. Otherwise there might occur artifacts in the circular component which are not existent, but originate from radial components being measured in a radially uncentered grid.

#### 4.4.2. Contribution to Sound Pressure

A second form of decomposition can be utilized to identify the regions on the loudspeaker which effectively contribute to the total radiated sound

pressure at a certain model point. The idea is to separate a vibration component which supports the sound radiation from a component which counteracts the sound vibration and a component which has no effect on the radiated sound at all.

The criterion to distinguish these three components is the phase relation between the vibration of each point on the cone surface and the total sound pressure at the model point. The vibration can be aligned with the total sound pressure in-phase, in anti-phase or out-of-phase.

$$\bar{x}_{total} = \bar{x}_{in} + \bar{x}_{anti} + \bar{x}_{out-of} \quad (0.9)$$

The phase of the displacement at each point on the surface is set in relation to a reference phase  $\varphi_{ref}$  starting from the phase of the total sound pressure  $\varphi_{ptotal}$  and including the time delay for the acoustical wave having traveled from the cone surface to the model point  $i$ .

$$\varphi_{ref,i} = \varphi_{ptotal} + k_0 |\bar{R}_i| + \pi \quad (0.10)$$

An additional phase shift of  $\pi$  origins from the phase difference between the displacement and the acceleration of the surface.

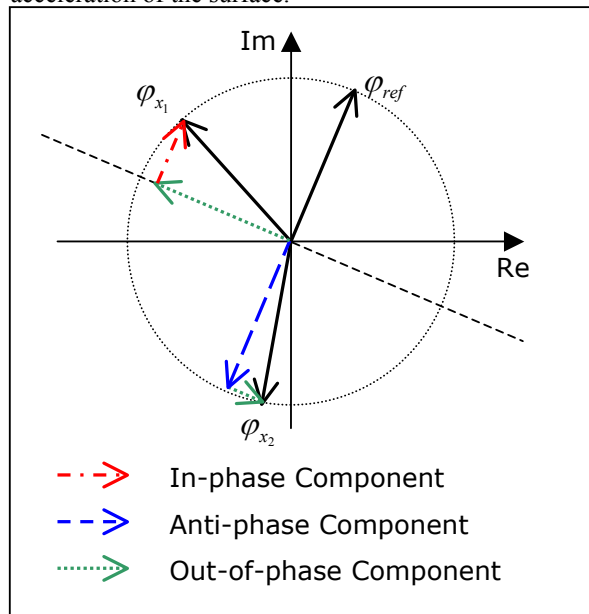


Fig. 26: Decomposition related to the radiated sound pressure.

An in-phase contribution describes now the positively related component between the phase of the displacement at each point  $\varphi_x$  and the reference phase  $\varphi_{ref}$ . The anti-phase component is accordingly the negatively related component and the out-of-phase component describes the component perpendicular to the total sound.

$$\bar{x}_{in-phase} = \text{Re}^+ \left\{ \hat{x} \frac{e^{j\varphi_x}}{e^{j\varphi_{ref}}} \right\} e^{j\varphi_{ref}} \quad (0.11)$$

$$\bar{x}_{anti-phase} = \text{Re}^- \left\{ \hat{x} \frac{e^{j\varphi_x}}{e^{j\varphi_{ref}}} \right\} e^{j\varphi_{ref}} \quad (0.12)$$

$$\bar{x}_{out-of-phase} = \text{Im} \left\{ \hat{x} \frac{e^{j\varphi_x}}{e^{j\varphi_{ref}}} \right\} e^{j\left(\varphi_{ref} + \frac{\pi}{2}\right)} \quad (0.13)$$

Having the possibility of decomposing the vibrations with respect to their contribution to the radiated sound offers many opportunities for analyzing the behavior of the measured loudspeaker. The in-phase component provides a clear picture, which cone regions effectively produce the sound pressure at a certain frequency.

## 5. INTERPRETATION

### 5.1. Piston Mode

At low frequencies most of the points of the cone and surround vibrate in phase and there are no waves propagating in radial direction as shown in Fig. 27. However, we may find circular modes producing standing waves at frequencies where a circular path is exactly two or more wavelengths long. Since the bending stiffness of the surround is much smaller than the stiffness of the cone the first circular waves usually occur on the surround at very low frequencies.

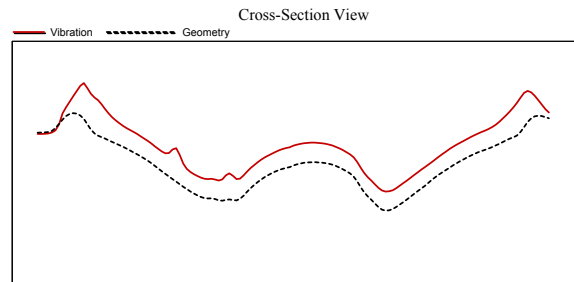
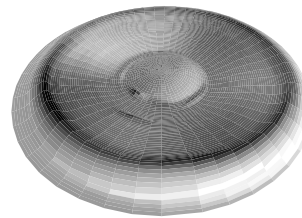


Fig. 27: Amplitude of the total vibration at 580 Hz.

Since the piston mode is still dominant in amplitude the decomposition technique is required to make smaller circular modes visible. The circular modes may be initiated by the wires and by a not even mass distribution on the cone and surround. The circular modes have not much influence on the sound radiation because the parts of the cone moving in anti-phase are so close together at those frequencies that their effect cancels out in the total volume velocity.

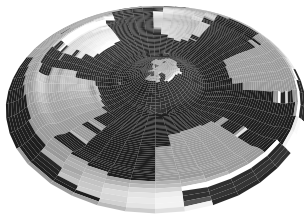


Fig. 28: Phase pattern of the out-of-phase vibration component at 580 Hz.

Fig. 28 shows the phase of the vibration component which is "acoustically short-circuited" and does not contribute to the sound pressure at the measurement point (1 m, in axis). This "out-of-phase" component contains only circular modes which generates black and white spots of similar size vibrating with opposite phase.

Although, the circular modes are not important for the sound radiation the first circular mode of the surround may cause a significant rocking mode and a rubbing of the coil in the gap.

## 5.2. Ring Resonance

At higher frequencies the vibration of the outer edge of the cone becomes higher and the vibration of the apex smaller. Fig. 29 shows the amplitude of the total vibration at 796 Hz. The total volume velocity generated by the cone and surround is approximately the same as in the piston mode and the sound pressure level at 1 m distance does not change significantly.

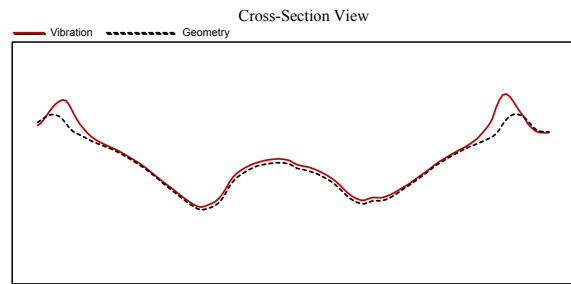
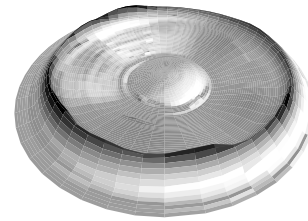


Fig. 29: Amplitude of the total vibration at 796 Hz.

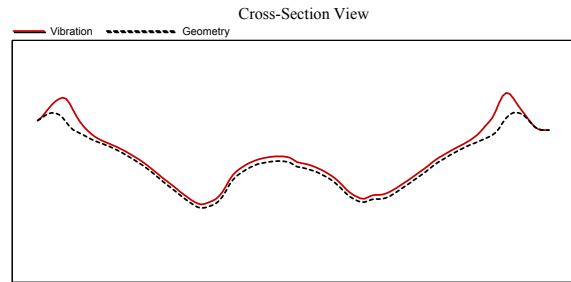
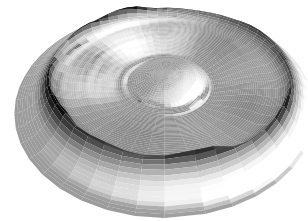


Fig. 30: Amplitude of the in-phase vibration component at 796 Hz.

Since all points of the cone and surround vibrate in phase the in-phase vibration component as shown in Fig. 30 is almost identical with the total vibration as shown in Fig. 29.

Fig. 31 shows the predicted sound pressure level at 1 m distance in axis ( $\theta=0$ ) which equals with the sound pressure radiated by the in-phase component up to 800 Hz. The sound pressure radiated by the anti-phase component is negligible.

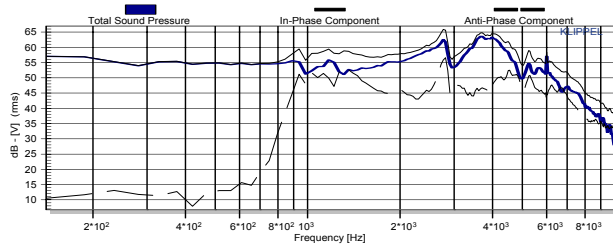


Fig. 31: Predicted sound pressure at 1 m in axis compared with the sound pressure generated by the in-phase and anti-phase component.

### 5.3. Surround Resonance

At a slightly higher frequency (984 Hz) the surround starts vibrating in anti-phase to the ring zone at the outer edge of the cone.

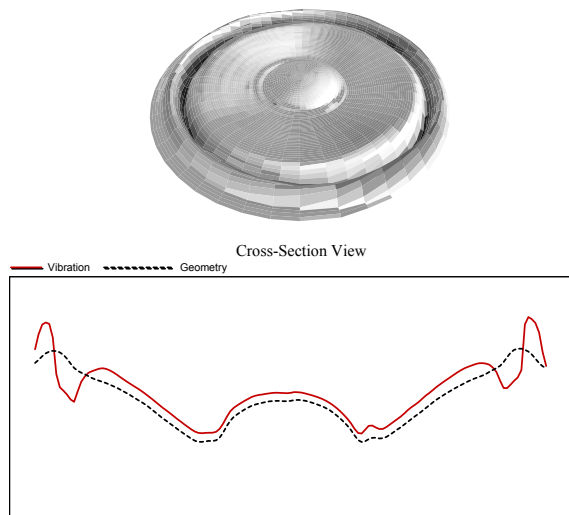


Fig. 32: Amplitude of the total vibration at the surround resonance 984 Hz.

If the volume velocity radiated by the surround (depending on the size of the surround and the displacement) equals the volume velocity radiated by the ring zone of the cone this resonance will radiate not much sound. This can be verified by separating the vibration components according their contribution to the sound pressure at the measurement point.

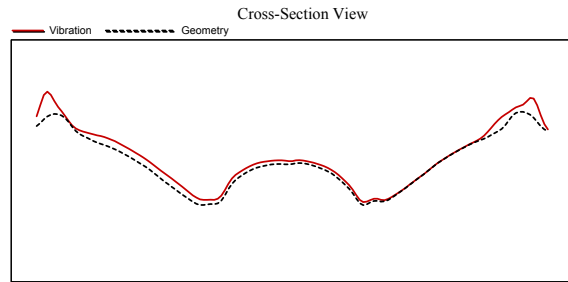
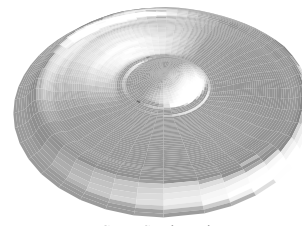


Fig. 33: Amplitude of the in-phase vibration component at the surround resonance (984 Hz).

The in-phase vibration component as shown in Fig. 33 shows a piston-like vibration of the inner cone part. The amplitude is relatively small but all points contribute equally to the radiated sound pressure. Fig. 31 shows that this component produces a sound pressure level which equals the value found at low frequencies. The bending mode of the surround and outer ring zone is almost not visible in the in-phase component.

The bending mode at the surround resonance can be found in the out-phase-component as shown in Fig. 34. This component reveals a significantly higher amplitude (> 15 dB) of the points at the outer ring zone and surround which does not radiate any sound.

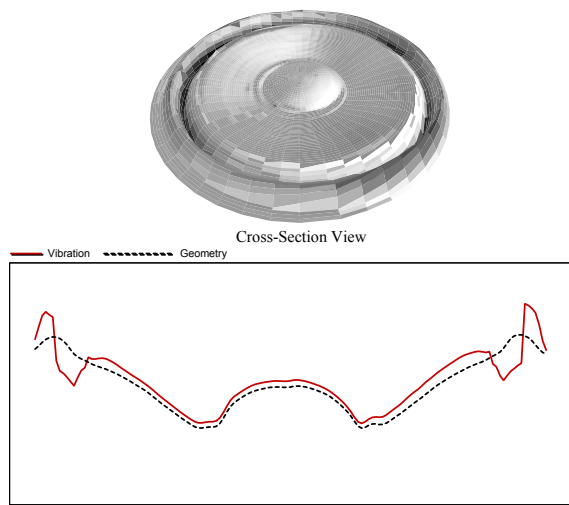


Fig. 34: Amplitude of the out-of-phase vibration component at the surround resonance (984 Hz).

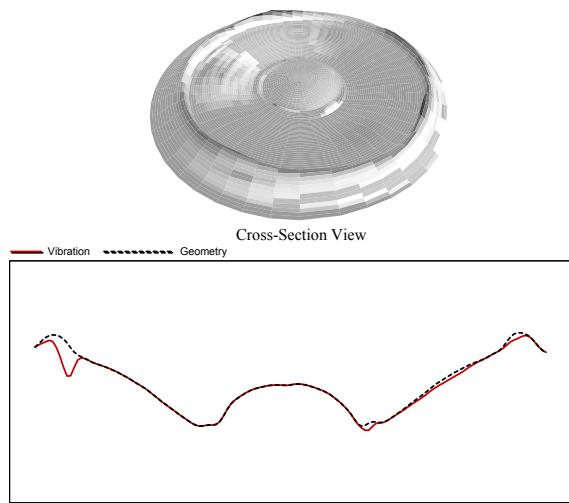


Fig. 35: Amplitude of the anti-phase vibration component at the surround resonance (984 Hz).

At the surround resonance there is also an anti-phase vibration component which directly reduces the sound radiation. This component has the highest displacement at points located at the outer ring zone of the cone. Fig. 31 shows that this component alone would generate a sound pressure level which is about 2 dB lower than the level of the total vibration. Thus this component reduces the sound pressure level generated by the in-phase component by 4 dB. The characteristic dip in the frequency response at 984 Hz can be reduced by changing the size of the surround.

#### 5.4. Transitional Region

Above the surround resonance more and more bending modes break up at the outer side of the cone. Fig. 36 shows the total vibration of the second bending mode at 3067 Hz. The inner part of the cone still vibrates as a rigid body and generates the sound pressure in the far field as shown in Fig. 37. The out-of-phase component in Fig. 38 comprises the bending motion which shows significant displacement but radiates no sound into the far field in axis.

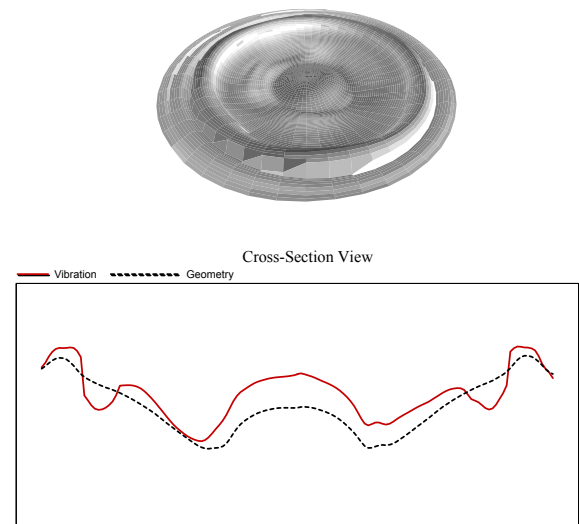


Fig. 36: Amplitude of the total vibration at 3046 Hz.

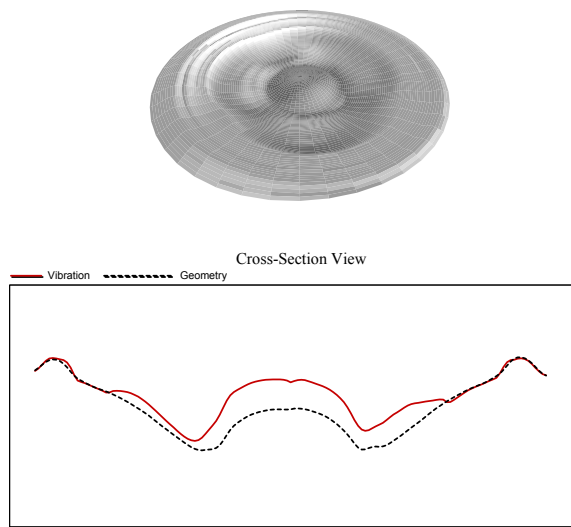


Fig. 37: Amplitude of the in-phase vibration component at 3046 Hz which generates the sound pressure in axis.

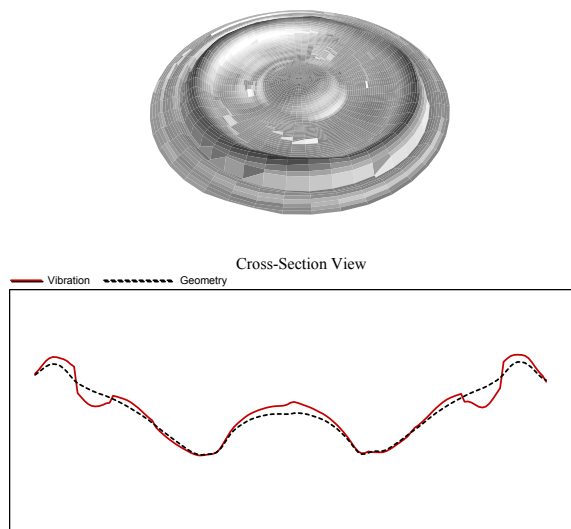


Fig. 38: Amplitude of the out-of phase vibration component at 3046 Hz which does not contribute to the sound pressure in axis.

At slightly higher frequencies parts of the bending motion also contributes to the sound pressure

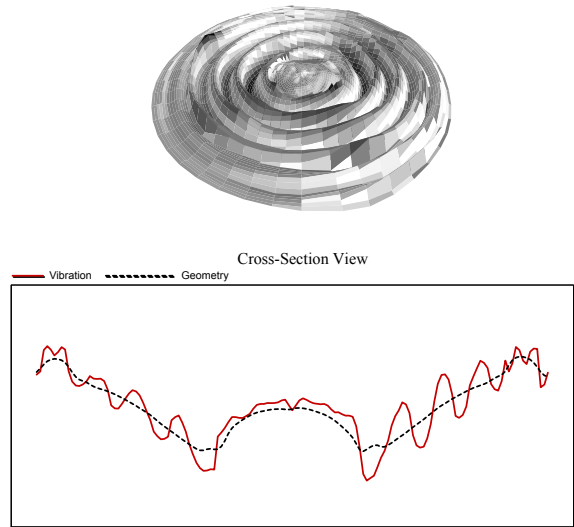


Fig. 39: Amplitude of the total vibration in the 7640 Hz.

At a frequency of 7640 Hz the whole cone is covered by bending modes as shown in the total vibration pattern in Fig. 40. Only a small ring at the inner part generates the sound pressure in axis.

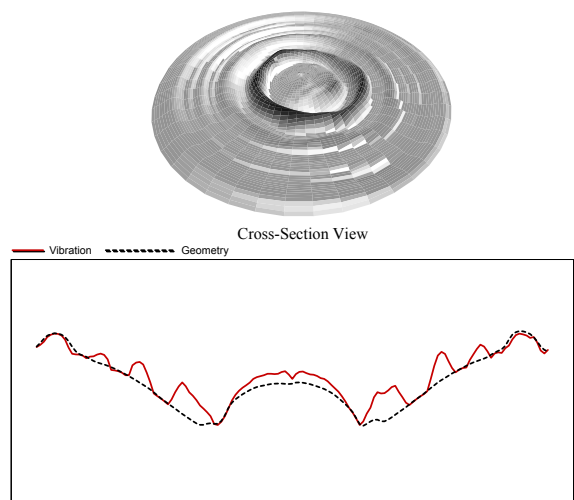


Fig. 40: Amplitude of the in-phase vibration component at 7640 Hz which generates the sound pressure in axis.

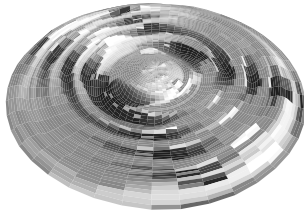


Fig. 41: Phase of the in-phase vibration component at 7640 Hz which generates the sound pressure at a point out of axis (1 m angle of 50 degree).

Since the phase decomposition technique considers the sound radiation conditions the in-phase vibration component varies with position of the model point in the sound field. For example Fig. 41 shows the separated in-phase component for a receiving point which is 50 degree out of axis. Under those condition not concentric rings vibrating at the same phase contribute to the sound pressure but the superposition of the phase of the vibrating point and its distance to the receiving point becomes important for the radiation.

## 6. CONCLUSIONS

A cost-effective laser scanning system can be realized by using a triangulation laser. A new decomposition technique simplifies the interpretation of the measured vibration data. Thereby the in-phase vibration component is most relevant, because it is directly related to the radiated sound pressure. In comparison to an FEA, the decomposition technique does not require any information about structural or material properties of the membrane, but it is only based on the measured phase relation. It can be used for the analysis and diagnostics of existing loudspeaker systems and support the development process for new prototypes. It is also interesting to note that the decomposition can be applied as well to the results of an FEA leading to new insights in the radiation behaviour of modelled loudspeakers.

## 7. REFERENCES

- [1] F.J.M. Frankort, "Vibration Patterns and Radiation Behavior of Loudspeaker Cones," J. of Audio Eng. Soc., Sept. 1978, Vol. 26, pp. 609- 622.
- [2] C. Struck, "Analysis of the Nonrigid Behavior of a Loudspeaker Diaphragm using Modal Analysis," presented at 86<sup>th</sup> convention of Audio Eng. Soc., Hamburg, 1989, preprint 2779.
- [3] A. J. M. Kaizer, A. D. Leeuwstein, " Calculation of the Sound Radiation of a Nonrigid Loudspaker Diaphragm Using the Finite-Element Method," J. Audio Eng. Soc., Vol. 36, No. 7/8, 1988 July/August, pp. 539 –551.
- [4] D. A. Barlow, et. al., " The Resonances of Loudspeaker Diaphragms," presented at the 65<sup>th</sup> Convention of the Audio Eng. Soc., February 1980, preprint 1590.
- [5] T. Heed, "Minimizing the Amplitude of Transverse Modal Waves in Diaphragms," presented at the 101<sup>st</sup> Convention of the Audio Eng. Soc., November 1996, Los Angeles, preprint 4333.